Expanded View Figures

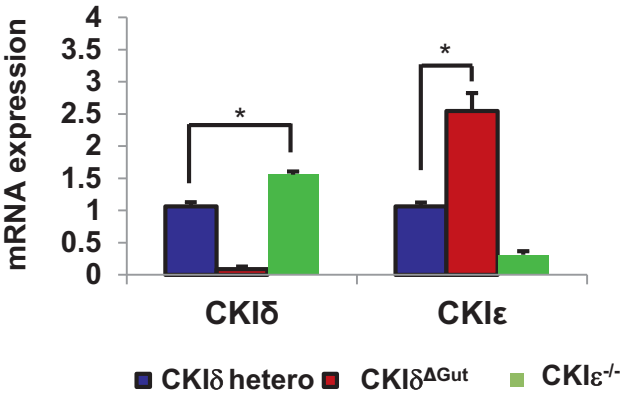

Figure EV1. Functional redundancy between CKIδ and CKIε in the gut.

qRT–PCR analysis of CKIδ and CKIε in IECs isolated from CKIδ$^{+/fl\ ER}$ (CKIδ hetero, $n = 3$), CKIδ$^{\Delta Gut}$ ($n = 3$), and CKIε$^{-/-}$ mice ($n = 3$, mean ± SEM); t-test was performed, $^*P < 0.05$.

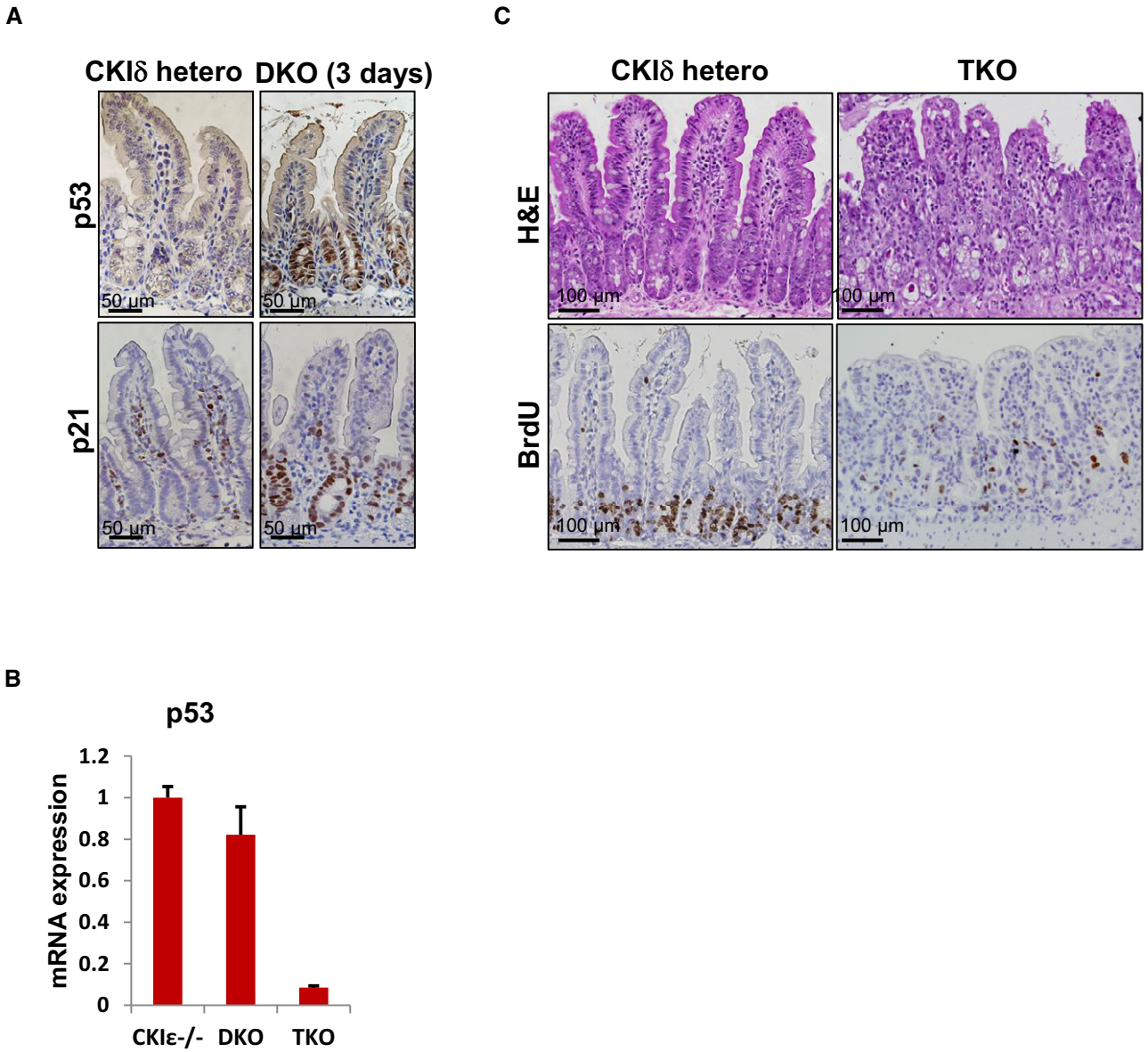

Figure EV2. CKIδ/ε ablation triggers a p53-independent cell cycle arrest.

A IHC analysis of p53 and p21 in intestinal sections from CKIδ hetero and DKO mice, 3 days after KO induction. Scale bar, 50 μm.

B qRT–PCR analysis of p53 levels after KO induction in CKIε$^{-/-}$, DKO, and CKIδ/ CKIε/p53 triple KO mice (TKO) (n = 3, mean ± SEM).

C H&E and IHC of BrdU in intestinal sections from CKIδ hetero and CKIδ/ CKIε/p53 triple KO mice (TKO), 5 days after KO induction. Scale bar, 100 μm.

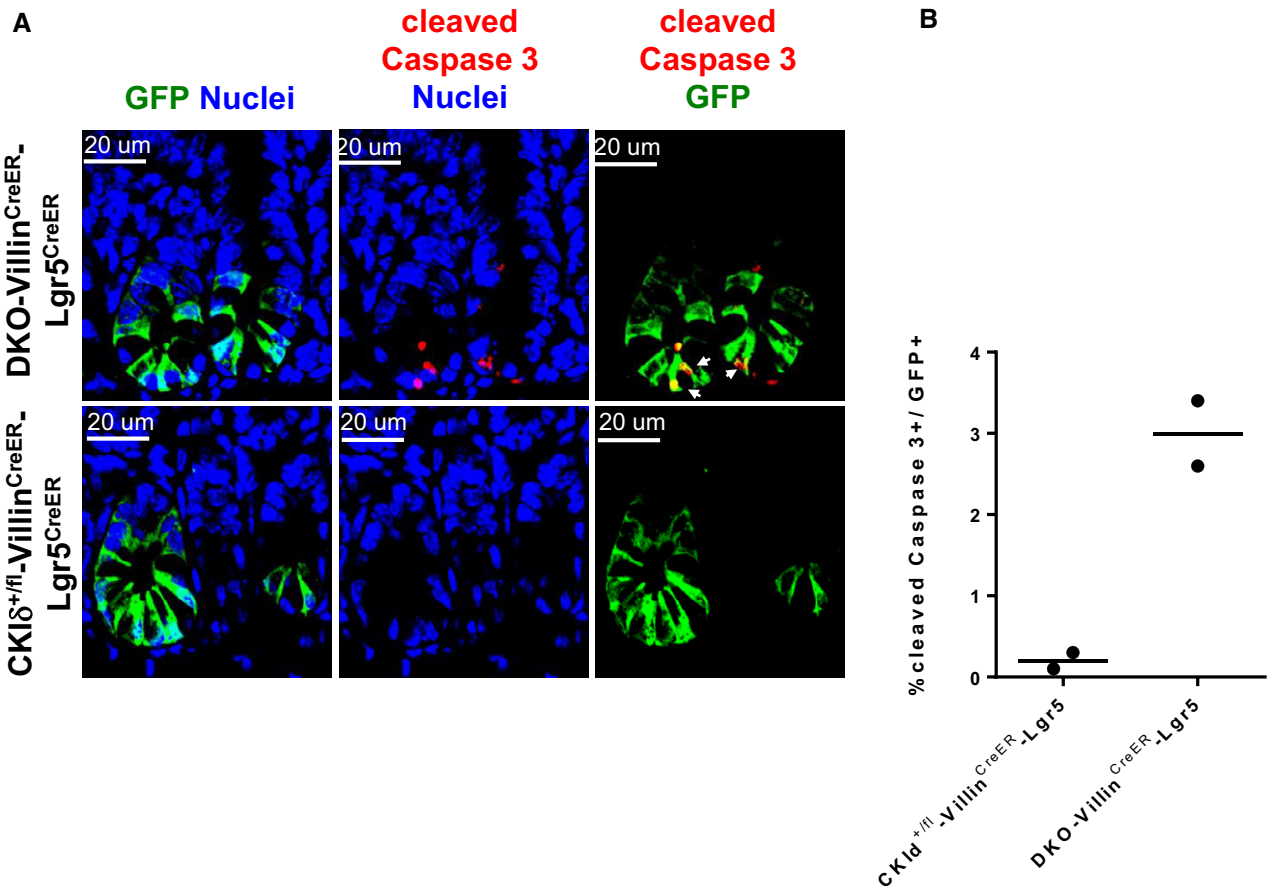

Figure EV3. CKIδ/ε depletion induces ISC apoptosis.

A IF analysis of GFP (green) and cleaved Caspase 3 (red) in intestinal sections of CKIδ$^{+/fl}$-Villin^{CreER}-Lgr5^{CreER} and DKO-Villin^{CreER}-Lgr5^{CreER} mice 3 days after KO induction; nuclear counterstain Hoechst. Scale bar, 20 μm. Arrows point to cells doubly stained by GFP and cleaved Caspase 3 representing apoptotic Lgr5-GFP cells.

B Quantification of cleaved Caspase 3 IF staining, based on %cleaved Caspase 3$^+$ cells out of 300 GFP$^+$ cells in CKId$^{+/fl}$-Villin^{CreER}-Lgr5^{CreER} (n = 2) and DKO-Villin^{CreER}-Lgr5^{CreER} mice (n = 2).

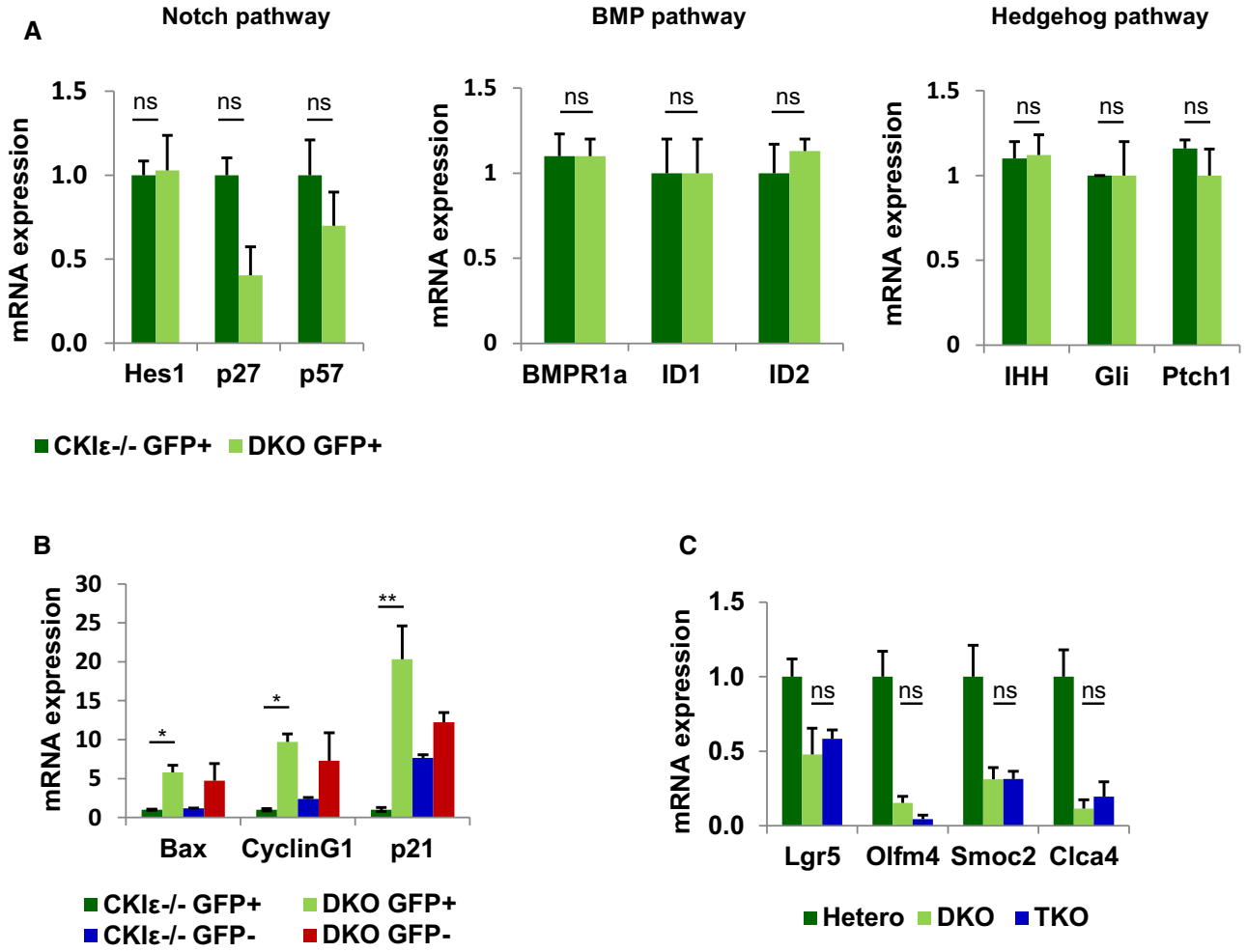

Figure EV4. Extinction of DKO ISCs is not mediated by Notch signaling downregulation or p53 activation.

A qRT–PCR analysis of Notch, BMP, and Hedgehog target genes in sorted GFP$^+$ cells isolated from crypts of CKIε$^{-/-}$-Villin^{CreER}-Lgr5^{CreER} (CKIε$^{-/-}$) and DKO-Villin^{CreER}-Lgr5^{CreER} mice (DKO) 2.5 days after KO induction. Data represent mean of three independent sorting experiments, each with a pool of six mice; *t*-test was performed, ns = non-significant. Error bars indicate SEM.

B qRT–PCR analysis of p53 targets in sorted GFP$^+$ and GFP$^-$ cells isolated from crypts of CKIε$^{-/-}$-Villin^{CreER}-Lgr5^{CreER} (CKIε$^{-/-}$) and DKO-Villin^{CreER}-Lgr5^{CreER} (DKO), 2.5 days after KO induction. Data represent mean of three independent sorting experiments, each with a pool of six mice; *t*-test was performed, $*P < 0.05$ $**P < 0.01$. Error bars indicate SEM.

C qRT–PCR analysis of ISC markers in IECs isolated from CKIδ hetero (hetero; $n = 3$), DKO ($n = 3$) and TKO ($n = 3$) mice (mean ± SEM), 5 days after KO induction; *t*-test was performed, ns = non-significant.

Figure EV5. Decreased levels of Dvl2 in crypt DKO IECs.

A Survival analysis was done by scoring 100 organoids of CKIε$^{-/-}$ and DKO organoids treated with ENR or ENR+VC. Data represent mean ± SEM of three independent experiments.

B Western blot analysis of nuclear (N) and cytoplasmatic (C) fractions of CKIε$^{-/-}$ and DKO mouse crypt IECs; p-Dvl2 identified by electrophoretic shift in Dvl mobility. WB quantification shown at the bottom.

C qRT–PCR analysis of Dvl isoforms in sorted GFP$^+$ cells isolated from crypts of WT, CKIε$^{-/-}$, CKIδ KO, and DKO mice 2.5 days after KO induction. Data represent mean of three independent sorting experiments, each with a pool of six mice.

D qRT–PCR analysis of Fzd isoforms in WT, CKIε$^{-/-}$, DKO, CKIε$^{-/-}$ Dvl-NLS, and DKO Dvl-NLS expressing organoids 4 days after tamoxifen treatment and KO induction ($n = 3$, mean ± SEM).

E Representative bright field images of CKIε$^{-/-}$ and DKO organoids expressing Dvl-NLS and shFzd7 at day 4 or 5 after KO and Dvl induction. Insets represent organoids counted as live. Scale bar, 400 μm.

Source data are available online for this figure.

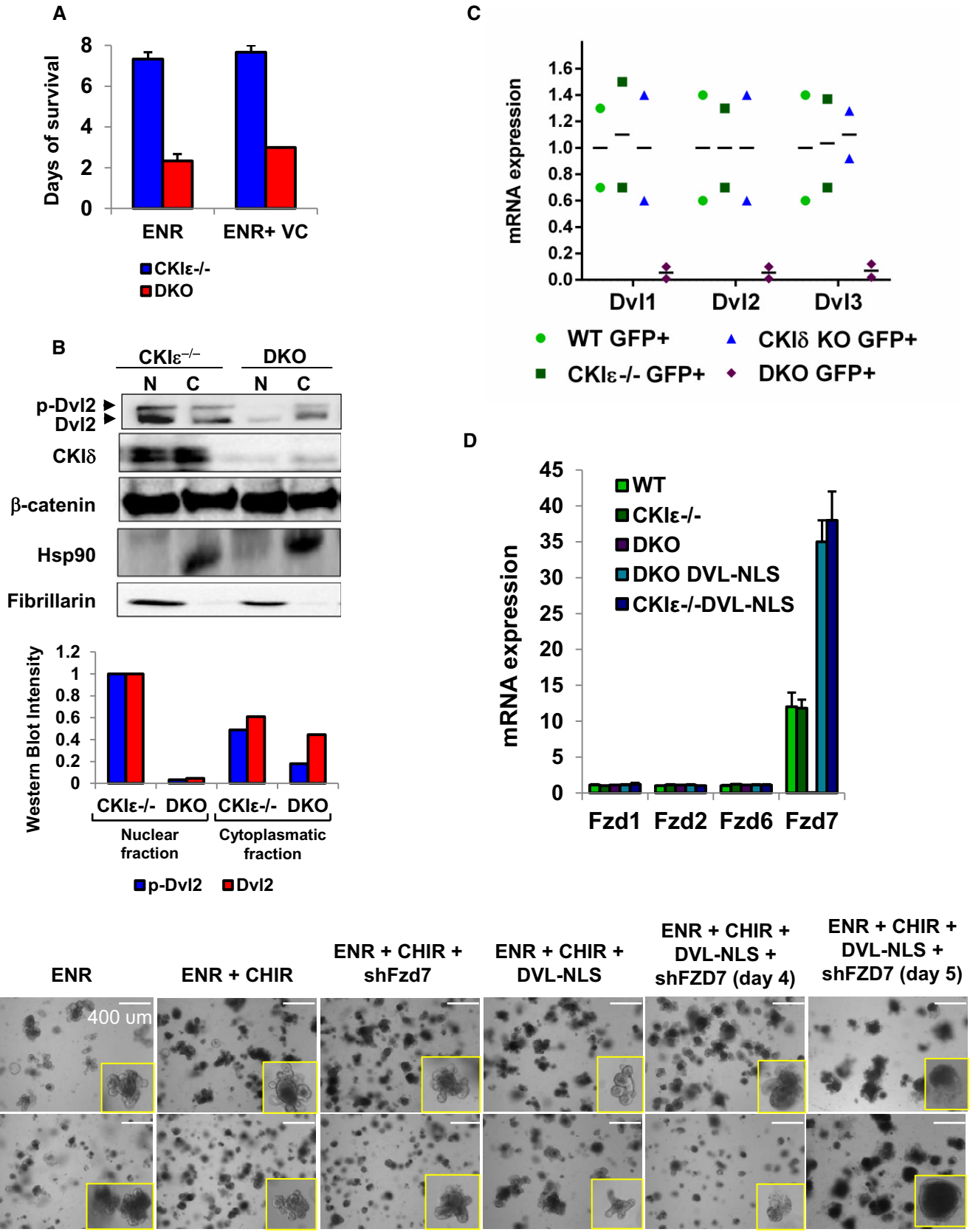

Figure EV5.

